Monthly Notices
of the
ROYAL ASTRONOMICAL SOCIETY

Mon. Not. R. Astron. Soc. **405,** 1195–1202 (2010) doi:10.1111/j.1365-2966.2010.16522.x

Calculation of rate constants for vibrational and rotational excitation of the H_3^+ ion by electron impact

Viatcheslav Kokoouline,[1,2⋆] Alexandre Faure,[3] Jonathan Tennyson[4] and Chris H. Greene[5]

[1]*Department of Physics, University of Central Florida, Orlando, FL 32816, USA*
[2]*Laboratoire Aimé Cotton, CNRS, Université Paris 11, 91405 Orsay, France*
[3]*Laboratoire d'Astrophysique, UMR 5571 CNRS, Université Joseph-Fourier, B.P. 53, 38041 Grenoble cedex 09, France*
[4]*Department of Physics and Astronomy, University College London, Gower Street, London WC1E 6BT*
[5]*Department of Physics and JILA, University of Colorado, Boulder, CO 80309, USA*

Accepted 2010 February 12. Received 2010 January 19

ABSTRACT

We present theoretical thermally averaged rate constants for vibrational and rotational (de-)excitation of the H_3^+ ion by electron impact. The constants are calculated using the multichannel quantum-defect approach. The calculation includes processes that involve a change $|\Delta J| \leq 2$ in the rotational angular momentum J of H_3^+. The rate constants are calculated for states with $J \leq 5$ for rotational transitions of the H_3^+ ground vibrational level. The thermal rates for transitions among the lowest eight vibrational levels are also presented, averaged over the rotational structure of the vibrational levels. The conditions for producing non-thermal rotational and vibrational distributions of H_3^+ in astrophysical environments are discussed.

Key words: molecular data – molecular processes – plasmas – ISM: molecules.

1 INTRODUCTION

Rotational and vibrational excitation of small polyatomic ions by electron impact is one of the important processes occurring in a neutral molecular plasma. In particular, the probability of rovibrational (de-)excitation in electron–ion collisions can be relatively high. The high probabilities and correspondingly high rate constants are driven by the non-Born–Oppenheimer coupling between electronic and rovibrational motions of the ion–electron system. In certain small polyatomic molecules, the coupling is particularly strong, as is the case for the H_3^+ ion.

Owing to its importance in interstellar space (Oka 2006), planetary ionospheres (Miller et al. 2000) and laboratory experiments (Larsson 2000; Plasil et al. 2002; Johnsen 2005), the H_3^+ ion has been studied for many years. In particular, processes involving electron scattering from the ion have been recently studied experimentally and theoretically. Such processes include electron-impact rovibrational excitation (Faure & Tennyson 2002; Faure et al. 2006a, 2009), dissociative recombination (Larsson 2000; Kokoouline, Greene & Esry 2001; Johnsen 2005; Fonseca dos Santos, Kokoouline & Greene 2007), electronic excitation and ionization (Gorfinkiel & Tennyson 2004), and photoionization (Bordas & Helm 1991; Stephens & Greene 1994, 1995; Mistrík et al. 2000; Kokoouline & Greene 2004a) of the metastable neutral H_3 molecule. Astrophysically, electron-impact excitation of molecular ions has been observed to be the dominant collisional excitation process in some environments (e.g. Jimenez-Serra et al. 2006).

Previously, cross-sections and rate constants for a few rotational transitions in H_3^+ have been calculated (Faure & Tennyson 2002, 2003; Kokoouline & Greene 2003b; Faure et al. 2006a,b). Vibrational rate constants have apparently not been studied extensively for this fundamental ion. Here, we present thermal rate constants for transitions between different rotational states of the ground vibrational level of H_3^+ with low angular momentum, $J \leq 5$. We also present thermal rate constants for rotationally averaged transitions between different vibrational levels.

The next section of the article briefly discusses the theoretical approach used in the present calculation. A detailed description of the approach is lengthy and has already been published elsewhere (Kokoouline & Greene 2003b; Fonseca dos Santos et al. 2007). Therefore, we only sketch here the main ideas of the approach. In Section 3, we present the rates for vibrational (de-)excitation of H_3^+. Section 4 is devoted to the calculation of rotational rate constants for transitions within rotational manifold of the ground vibrational level. Astrophysical implications are discussed in Section 5. Finally, Section 6 presents our conclusions.

2 THEORETICAL APPROACH

The theoretical model employed in the present study is based on quantum-defect theory. It is discussed in detail by Kokoouline & Greene (2003a), Kokoouline & Greene (2003b), Faure et al. (2006a)

⋆E-mail: slavako@mail.ucf.edu

and Fonseca dos Santos et al. (2007). Here, we only mention the main ideas used in the model.

The energy-dependent theoretical rate constant $\alpha_{i'\leftarrow i}(E)$ for a transition from the initial rovibrational level i to a final one i' is obtained from the corresponding matrix element $S^{\rm phys}_{i'i}(E)$ of the energy-dependent scattering operator, $\hat{S}^{\rm phys}(E)$. The main difficulty in the theoretical approach is the construction of the scattering matrix $S^{\rm phys}_{i'i}(E)$, (the indices i and i' refer to specific rovibrational states of the H_3^+ ion; the electron angular momentum and its coupling with the ion to form a total angular momentum eigenstate are implied as well, but these will be suppressed in our notation since they are diagonal quantum numbers in the present approximation). For our discussion, it is convenient to represent the index i as rv, where $r = (JK)$ specifies the rotational quantum numbers, i.e., ionic angular momentum J and its projection K on the molecular axis and $v = \{v_1, v_2^{l_2}\}$ specifies the vibrational quantum numbers in a normal-mode classification. We note that our model neglects the explicit coupling between rotational and vibrational angular momenta which occur for excited vibrational states with $l_2 > 0$ and which leads to a more complicated set of quantum numbers (Lindsay & McCall 2001).

The construction of the scattering matrix $S^{\rm phys}_{i'i}(E)$ begins from the *ab initio* potential surfaces of the ground electronic state of the ion and several excited states of the neutral H_3 molecule (Mistrík et al. 2000), [$U^+(\mathcal{Q})$ for the ion and $U_n(\mathcal{Q})$ for the neutral molecule]. We will use the symbol $\mathcal{Q}$ to specify collectively the three internuclear distances. For a given geometry $\mathcal{Q}$, the electronic wavefunction of the outer electron of the H_3 excited states resembles the electronic wavefunction of the hydrogen atom. However, due to the fact that at short distances from the ionic core, the electron–ion interaction is different from that in the hydrogen atom; the electron binding energy $U^+(\mathcal{Q}) - U_n(\mathcal{Q})$ is generally different from the corresponding binding energy $1/(2n^2)$ in the hydrogen atom (n is the principal quantum number). The departure of the $U^+(\mathcal{Q}) - U_n(\mathcal{Q})$ difference from $1/(2n^2)$ is written as $1/(2(n-\mu)^2)$, where the quantum defect μ is only weakly dependent on the principal quantum number n. When the energy E of the electron+ion system approaches the ionization limit ($n \to \infty$) and becomes larger, the principal quantum number n loses its physical meaning, but the quantum defect μ does not: it gives the collisional phase shift $\delta(E) = \pi\mu$ in terms of the scattering phase in electron–ion collisions at energies above the ionization limit (Seaton 1966). The phase shift also depends weakly on the energy E and it determines the scattering matrix $S(E) = \exp(2i\delta)$. This is the reason why the energies of excited electronic states in the neutral molecule can be used to obtain the quantum defect and to describe collisions between the ion and the electron.

The preceding discussion assumes that the electron scatters from (or is bound to) the molecular ion, which stays at a given geometry, i.e., the nuclei remain fixed throughout. This approximation is only reliable on a time-scale much shorter than the period of ionic vibrational motion. In this limit, the quantum defects are functions of geometry $\mathcal{Q}$, $\mu(\mathcal{Q})$. Generally speaking, the dependence of $\mu(\mathcal{Q})$ is much smoother than the dependence of $U^+(\mathcal{Q})$ and $U(\mathcal{Q})$. Although the quantum defect depends only weakly on the principal quantum number n, it usually depends strongly on the angular momentum l and on its projection Λ on the molecular axis of the ionic core. For a non-linear triatomic ion such as H_3^+, the body-frame quantization axis is chosen as the normal to the plane containing the nuclei. At large $l \geq 2$, the quantum defects become small, because the electronic wavefunction of high l approaches the unperturbed wavefunction in the hydrogen atom.

Therefore, for the description of an electron–ion scattering process involving low values of l, one must obtain the quantum-defect functions $\mu_{l\Lambda}(\mathcal{Q})$ for various l and Λ and the corresponding scattering matrices $S(\mathcal{Q}) = \exp(2i\delta_{l\Lambda})$. The calculated potential energy surfaces are obtained in the Born–Oppenheimer approximation (Mistrík et al. 2000), i.e., in which the coupling between electronic and nuclear motion is neglected. The quantum defects and the scattering matrices obtained from the potential surfaces as described above, therefore, fail to account for the coupling. However, in the $H_3^+ + e^-$ case, a strong non-adiabatic Jahn–Teller interaction must be accounted for in order to appropriately describe the scattering process. It mixes the two π electronic states of the same orbital angular momentum l of the incoming electron and can be included in the scattering matrix built from quantum defects using the formalism suggested in Staib & Domcke (1990). The resulting scattering matrix is now not diagonal over the Λ quantum numbers. The strongest coupling is between the $p\pi$ electronic states. In our treatment, we include only p states (π and σ). This implies that this body-frame (BF) scattering matrix $S^{\rm BF}_{\Lambda',\Lambda}(\mathcal{Q})$ is a 3×3 matrix (Kokoouline & Greene 2003b).

The scattering matrix constructed in this way represents the electron–ion scattering only if the ion stays at the same configuration $\mathcal{Q}$ during the entire process, which is not a valid description. The physically meaningful scattering matrix must describe the amplitude of scattering from a particular rovibrational state of the ion to another one, including the possibility of nuclear motion during the full collision process. We denote this as the space-fixed (SF) scattering matrix $S^{\rm SF}_{s',s}$, where s and s' refer to initial and final states of the ion. The formalism of the rovibrational frame transformation (Atabek, Jungen & Dill 1974; Fano 1975; Jungen & Atabek 1977) allows us to use the matrix $S^{\rm BF}(\mathcal{Q})$ to construct the $S^{\rm SF}_{s',s}$ matrix. In this formalism, the two matrices are considered as two equivalent forms of the same scattering operator in two different representation bases. The representation basis of $S^{\rm SF}_{s',s} = \langle s'|\hat{S}|s\rangle$ is the set of rovibrational energy eigenstates $|s\rangle$. The basis for the $S^{\rm BF}(\mathcal{Q})$ matrix is made of tensor products $|b\rangle = |\mathcal{Q}\rangle|\Lambda\rangle$, where $|\mathcal{Q}\rangle$ represents the vibrational position eigenstates of the ion, $|\Lambda\rangle$ is the angular state vector of the electron in either the $p\pi$ or $p\sigma$ state.

The two representations are connected by the standard basis transformation formula

$$S^{\rm SF}_{s',s} = \sum_{b',b} \langle s'|b'\rangle \langle b'|\hat{S}|b\rangle \langle b|s\rangle \,, \tag{1}$$

where the summation indicates a sum over discrete indices and an integration over the continuous coordinates $\mathcal{Q}$, and rotational coordinates (three Euler angles). Because the scattering matrix in the $|b\rangle$ basis is diagonal over $|\mathcal{Q}\rangle$, it is convenient to write $\langle b'|\hat{S}|b\rangle$ as $S^{\rm BF}_{\Lambda',\Lambda}(\mathcal{Q})\delta(\mathcal{Q}-\mathcal{Q}')$, the notation that has already been used in the above discussion. The explicit form of the matrix elements $\langle s|b\rangle$ for the unitary transformation is given in Kokoouline & Greene (2004a,b).

The $S^{\rm BF}$ matrix is diagonal with respect to the rotational quantum numbers $J_{\rm tot}$, $K_{\rm tot}$ and $M_{\rm tot}$ of the whole molecule and the continuous coordinate $\mathcal{Q}$. $J_{\rm tot}$, $K_{\rm tot}$ and $M_{\rm tot}$ are the angular momentum of the neutral molecule and the two projections of the angular momentum on the molecular symmetry axis and on the space-fixed z-axis, respectively. To completely define the BF basis functions $|b\rangle$, in addition to Λ and $\mathcal{Q}$, the rotational quantum numbers $J_{\rm tot}$, $K_{\rm tot}$ and $M_{\rm tot}$ must also be specified; for brevity they are omitted in the above equation, although their presence is implied.

To specify the vibrational states in the SF representation, we will use the normal-mode approximation, i.e., specifying ionic

vibrational eigenstates by the quantum numbers $\{v_1, v_2^{l_2}\}$. The rotational part of the total wavefunction is specified by rotational quantum numbers $J_{\rm tot}$, J, K, M, l and m, where J, K and M are the angular momentum of the ion and the two projections of the angular momentum on the molecular symmetry axis and on the space-fixed z-axis, m is the projection of electronic angular momentum l on the space-fixed z-axis. In the following, we will not specify any other conserved quantum numbers that are the same in both bases, such as the total nuclear spin and the irreducible representation of the total wavefunction.

The matrix $S^{\rm SF}_{s',s}$ obtained by the above procedure does not yet represent the physical scattering matrix (Aymar, Greene & Luc-Koenig 1996; Seaton 1966). In fact, it represents the actual scattering matrix $S^{\rm phys}(E)$ only for energies high enough such that *all* of the channels $|s\rangle$ are open for electron escape, i.e., where the total energy of the system is higher than the energy of the highest relevant ionization channel $|s\rangle$. When at least one channel is closed, the physical scattering matrix $S^{\rm phys}(E)$ is obtained from $S^{\rm SF}$ using the standard Multi-channel Quantum Defect Theory (MQDT) channel-elimination formula (see equation 2.50 in Aymar et al. 1996 or equation 38 in Kokoouline & Greene 2004a).

In terms of the energy-dependent scattering matrix $S^{\rm phys}(E)$, the cross-section for rovibrational (de-)excitation of the ion from the initial state $|s\rangle$ is written (in atomic units, a.u.) as

$$\sigma^{\rm RFT}_{s'\leftarrow s}(E_{\rm el}) = \frac{\pi}{2E_{\rm el}(2J+1)} \sum_{J_{\rm tot}K_{\rm tot}} (2J_{\rm tot}+1)|S^{(J_{\rm tot},K_{\rm tot})}_{s',s}|^2, \qquad (2)$$

where $E_{\rm el}$ is the relative kinetic energy of the ion and the electron before the collision. In the above expression it has been assumed that the initial $|s\rangle$ and final $|s'\rangle$ states are different.

3 RATE CONSTANTS FOR VIBRATIONAL (DE-)EXCITATION

If one is not interested in the rotational structure of initial and final vibrational states, the final cross-section (or thermal rate constant) has to be averaged over the initial rotational levels and summed up over the final rotational levels. This can be done using the full rovibrational frame transformation technique described above. However, the cross-section averaged over initial rotational levels and summed up over the final rotational levels is very similar to the one obtained neglecting the rotational structure of the ion. The cross-section obtained accounting for the rotational structure has more resonances due to interaction between rotational states, but the averaged value is close to the value obtained without the rotational structure. The quantity of interest in astrophysical applications is the thermally averaged rate constant. Because the thermally averaged rate is not sensitive to the position of individual resonances in the energy-dependent cross-section, the calculations with and without the rotational structure give the same result.

Figs 1 and 2 compare our calculations with and without rotational structure included, for the probabilities of rovibrational and vibrational (de-)excitation of the ion. Fig. 1 shows in detail the rovibrational transitions from the ground to the first excited vibrational level $\{01^1\}$ with $J_{\rm tot} = 2$ in para-H_3^+. In order to compare with the results in Fig. 2, one would need to take a sum over final quanta and average over initial J and K, and account for all possible $J_{\rm tot}$ and $K_{\rm tot}$ similar as it is done in equation (2). This would mean that to achieve a converged result at reasonably high energy ($\sim$2000 cm^{-1}) calculations would be needed for all $J_{\rm tot}$ up to 10. This would require a tremendous numerical effort if the fully quantum approach was to be applied.

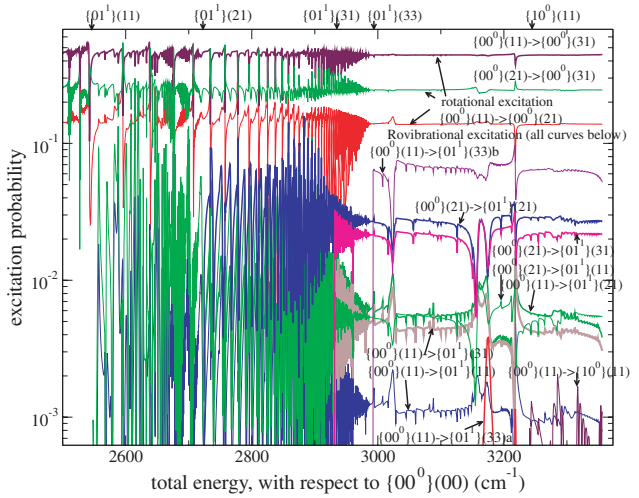

Figure 1. Probabilities of rovibrational excitation of the H_3^+ ion calculated using the full rovibrational frame transformation. Only transitions from the ground vibrational level $\{00^0\}$ are shown. The $\{00^0\} \rightarrow \{01^1\}$ probabilities oscillate a lot below 3000 cm^{-1} and become less energy-dependent above. The oscillations are due to the strong rotational coupling between individual rotational levels of the initial and final states of the ion. When averaged over the initial and summed over the final rotational states and averaged over the appropriate energy distribution, the resulting probabilities are similar in magnitude to the probabilities shown in Fig. 2. The labels on top of the figure indicate different rovibrational ionization limits. Note that the zero of energy in the figure is set to the energy of the forbidden rovibrational level $\{00^0\}(00)$.

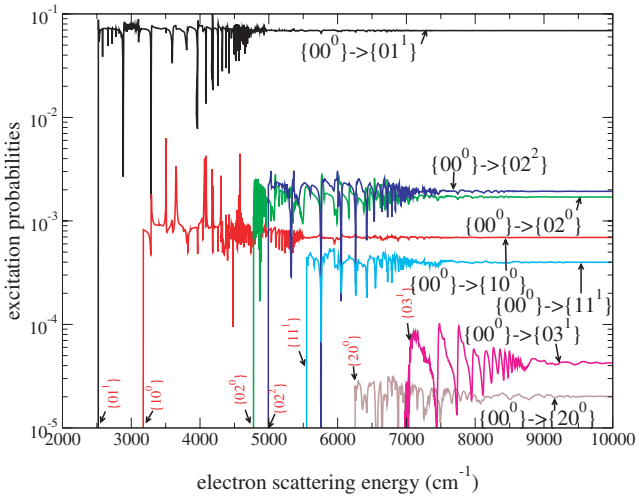

Figure 2. Probabilities of vibrational excitation from the ground vibrational level $\{00^0\}$ to several excited vibrational levels calculated using the vibrational frame transformation only. Energies of vibrational thresholds are labelled with arrows and the corresponding vibrational quantum numbers.

Neglect of the rotational structure of the initial and final vibrational state simplifies considerably the numerical calculation. The complete rovibrational frame transformation of equation (1) is reduced to the vibrational frame transformation if the rotation is neglected, i.e., it is carried out using the following formula

$$S^{\rm SF}_{(v'\Lambda')(v\Lambda)} = \left\langle v'|S^{\rm BF}_{\Lambda';\Lambda}(\mathcal{Q})|v\right\rangle, \qquad (3)$$

where the brackets imply an integration over the vibrational coordinates only. Many elements among $S^{\rm SF}_{(v'\Lambda')(v\Lambda)}$ are zero because of

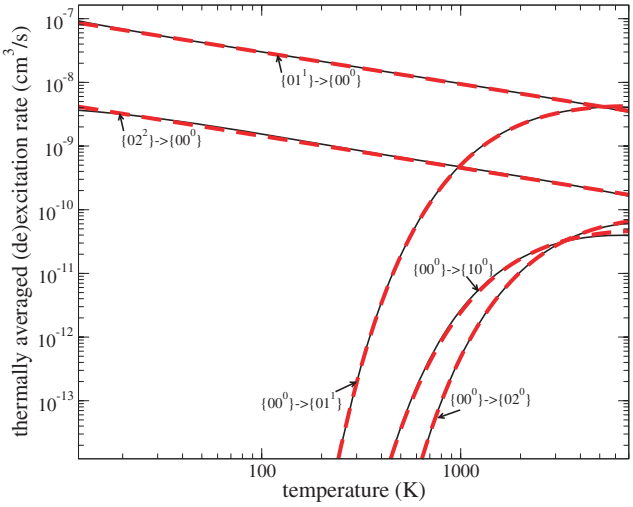

Figure 3. Thermally averaged rate constants for several (de-)excitation transitions obtained by direct integration using equation (4) (solid lines) and the approximate formula of equation (7) (dashed line). The averaged probabilities for vibrational (de-)excitations are listed in Table 1.

the symmetry of vibrational wave functions and matrix elements $S^{\rm BF}_{\Lambda'\Lambda}(\mathcal{Q})$. The vibrational (de-)excitation $v \rightarrow v'$ cross-section obtained from the scattering matrix of equation (3) should be averaged over Λ and summed over Λ'.

The thermally averaged rate constant $\alpha_{\rm th}(T)$ (in a.u.) is obtained from the energy-dependent cross-section $\sigma(E)$ as

$$\alpha_{\rm th}(T) = \frac{8\pi}{(2\pi kT)^{3/2}} \int_0^\infty \sigma(E_{\rm el}) {\rm e}^{-\frac{E_{\rm el}}{kT}} E_{\rm el} {\rm d}E_{\rm el}\,, \qquad (4)$$

where T is the temperature. Temperature dependencies $\alpha_{\rm th}(T)$ for different rovibrational transitions $v \rightarrow v'$ obtained using equation (4) are shown in Fig. 3 as solid lines.

For further discussion, it is convenient to represent the cross-section $\sigma(E_{\rm el})$ in the form

$$\sigma(E_{\rm el}) = \frac{\pi}{k^2} P(E_{\rm el})\,, \qquad (5)$$

where k is the wave vector of the incident electron, $P(E_{\rm el})$ is the probability for vibrational (de-)excitation at collision energy $E_{\rm el}$. Figs 1 and 2 suggest that on average (here we mean a running average taken over a few intervals between resonances), the probability behaves approximately as a step function

$$\langle P(E_{\rm el})\rangle = P_0 \theta(E_{\rm el} - \Delta_{v',v})\,, \qquad (6)$$

where $\Delta_{v'v} = E_{v'} - E_v$ is the threshold energy for rovibrational excitation (if $E_{v'} - E_v > 0$); $\Delta_{v'v} = 0$ for (de-)excitation (if $E_{v'} - E_v < 0$), θ is the Heaviside function, P_0 is a constant. The above approximation for the probability is accurate enough to calculate the thermally averaged rate constant that is not sensitive to the detailed resonance structure of the energy-dependent (de-)excitation cross-section. Using equation (6) the thermally averaged rate constant of equation (4) becomes

$$\alpha_{\rm th}(T) = \sqrt{\frac{2\pi}{kT}} {\rm e}^{-\frac{\Delta_{v'v}}{kT}} P_0\,. \qquad (7)$$

The above formula with only one parameter P_0 provides a very good approximation for the actual thermally averaged rate constant. It is demonstrated in Fig. 3 that compares the thermal rate constants for different (de-)excitation transitions obtained with the direct numerical integration using equation (4) and with the approximate formula of equation (7). Therefore, for practical applications, it is convenient to provide just averaged probabilities P_0 and the energies of vibrational thresholds E_v for each pair of vibrational (de-)excitations. These parameters are listed in Table 1 for all combinations of the first eight vibrational states of H_3^+. *Note that the conversion factor from a.u. to cm^3 s^{-1} is 6.126 × 10^{-9}.*

4 RATE CONSTANTS FOR ROTATIONAL (DE-)EXCITATION

If the temperature T of the $H_3^+ + e^-$ plasma is not very high, such that only the ground vibrational level $\{00^0\}$ of H_3^+ is significantly populated, knowledge of rate constants for transitions $r \rightarrow r'$ between individual rotational levels r and r' of $\{00^0\}$ may be important for the analysis of experimental or astronomical spectra. For this purpose, we have made a detailed analysis of transitions between individual rotational states of the ground vibrational level. The calculation of rotational (de-)excitation rate constants was carried out using the cross-section of equation (2) and numerical integration of equation (4). Examples of the thermally averaged rate constants for the rotational (de-)excitation are shown in Fig. 4.

As is evident from the figure, the rotational rate constants behave approximately according to equation (7), where $\Delta_{v'v}$ should be replaced with the rotational threshold energy, $\Delta_{r'r} = (E_{r'} - E_r)\theta(E_{r'} - E_r)$. However, there is a weak departure from the dependence of equation (7). It is clearer in Fig. 5, where we plotted an 'effective' value $P_{\rm eff} = \alpha_{r'\leftarrow r}(T)\sqrt{T}\exp(\frac{\Delta_{r'r}}{T})$ of the parameter P_0 as a function of $\ln(T)$. Notice that on average, the quantities $P_{\rm eff}[(J'K') \leftarrow (JK)]$ and $P_{\rm eff}[(JK) \leftarrow (J'K')]$ for the two

Table 1. Parameters P_0 for several vibrational transitions that can be used in the approximate formula, equation (7), for thermally averaged rate constants. Initial states v are given in the upper row, final states v' – in the left column. The upper row specifies also the energies E_v (in cm^{-1}) of vibrational levels. The probabilities P_0 are obtained by fitting numerical dependencies obtained by a direct integration of equation (4). That is why $P_0(v' \rightarrow v)$ is not exactly equal to $P_0(v \rightarrow v')$. Note that multiplicity factors of doubly degenerate vibrational states E are taken into account in the probabilities. For example, $P_0(v \rightarrow v') \approx 2P_0(v' \rightarrow v)$, if the vibrational states v and v' are the states of the A_1 and E irreducible representations correspondingly.

	$\{00^0\}$0	$\{01^1\}$2521	$\{10^0\}$3178	$\{02^0\}$4778	$\{02^2\}$4998	$\{11^1\}$5554	$\{20^0\}$6262	$\{03^1\}$7006
$\{00^0\}$		3.7×10^{-2}	8.5×10^{-4}	1.5×10^{-3}	1.1×10^{-3}	2.0×10^{-4}	2.3×10^{-5}	2.1×10^{-5}
$\{01^1\}$	6.9×10^{-2}		1.2×10^{-2}	6.0×10^{-2}	6.4×10^{-2}	3.3×10^{-3}	2.2×10^{-4}	3.6×10^{-3}
$\{10^0\}$	8.0×10^{-4}	5.7×10^{-3}		2.0×10^{-3}	5.9×10^{-4}	3.5×10^{-2}	1.4×10^{-3}	2.4×10^{-4}
$\{02^0\}$	1.7×10^{-3}	2.9×10^{-2}	1.9×10^{-3}		1.2×10^{-2}	3.5×10^{-3}	8.8×10^{-5}	4.3×10^{-2}
$\{02^2\}$	1.9×10^{-3}	6.3×10^{-2}	1.4×10^{-3}	3.0×10^{-2}		1.4×10^{-2}	1.7×10^{-4}	2.6×10^{-2}
$\{11^1\}$	3.9×10^{-4}	2.8×10^{-3}	7.1×10^{-2}	6.3×10^{-3}	1.3×10^{-2}		1.8×10^{-2}	2.3×10^{-3}
$\{20^0\}$	2.0×10^{-5}	1.0×10^{-4}	1.3×10^{-3}	6.7×10^{-5}	1.0×10^{-4}	1.1×10^{-2}		1.2×10^{-5}
$\{03^1\}$	4.3×10^{-5}	4.1×10^{-3}	6.3×10^{-4}	1.0×10^{-1}	2.8×10^{-2}	2.2×10^{-3}	2.8×10^{-5}	

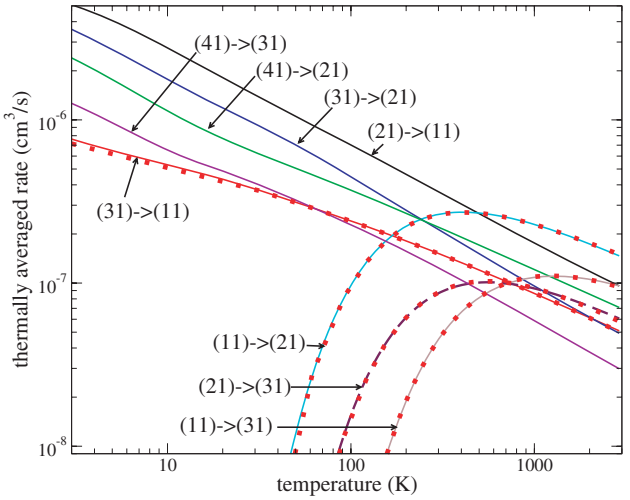

Figure 4. Thermally averaged rate constants for several rotational (de-)excitation transitions $(JK) \rightarrow (J'K')$ of the H_3^+ ion (solid lines). The vibrational level, $\{00^0\}$, is the same in the initial and final state of the ion. The dotted lines show a few examples of the numerical fit using equation (9).

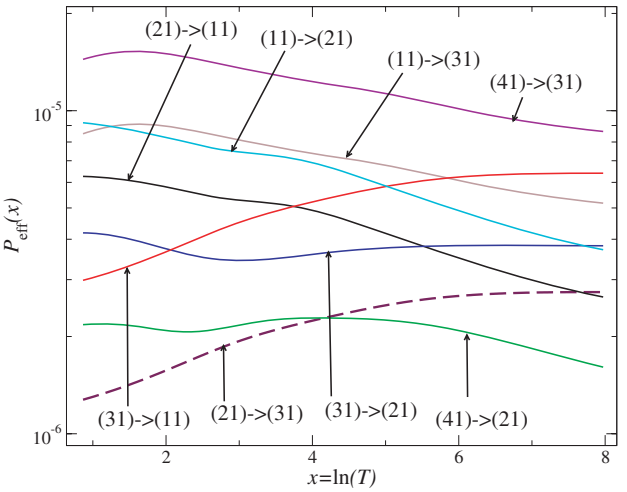

Figure 5. $P_{\rm eff} = \sqrt{T}\exp\left(\Delta_{r',r}/T\right)\alpha\left[J'K' \leftarrow JK\right]$. Note that $P_{\rm eff}$ is only weakly dependent on temperature. It is used to obtain a cubic polynomial fit $P_m[\ln(T)]$ in equation (9) for each transition $(JK) \rightarrow (J'K')$ with four parameters that are listed in Tables 2, 3, 4 and 5.

opposite processes are related by the principle of detailed balance

$$(2J+1)P_{\rm eff}[(J'K') \leftarrow (JK)] \approx (2J'+1)P_{\rm eff}[(JK) \leftarrow (J'K')], \tag{8}$$

because $P_{\rm eff}(x)$ represents the thermally averaged probability of the rotational transition per one electron–ion collision (see also equation 2). In order to simplify eventual applications of the calculated numerical constants $\alpha_{r',r}(T)$, we fitted the numerical rate constants representing the 'effective' value of P_0 in equation (7) to a cubic polynomial of $\ln(T)$. For this, we used the following analytical interpolation formula for $\alpha_{r',r}(T)$

$$\alpha_{r'\leftarrow r}(T) = \frac{1}{\sqrt{T}}\exp\left(-\frac{\Delta_{r'r}}{T}\right)P_m(x), \tag{9}$$

where $P_m(x) = a_0 + a_1x + a_2x^2 + a_3x^3$ and $x = \ln(T)$. The constants a_i $(i = 0, 1, 2, 3)$ are obtained for each individual transition $r \rightarrow r'$ from a numerical fit. The quantity $P_m(x)$ in the above equation has a meaning of (de-)excitation probability that varies weakly with energy. We used the subscript m to distinguish it from $P_{\rm eff}$ and to stress that $P_m(x)$ is given by a model polynomial. The constants obtained, a_i, are listed in Tables 2, 3, 4 and 5 for several combinations of initial $r = (J, K)$ and final $r' = (J'K')$ rotational states of H_3^+. The numerical values of a_i listed in the table are such that, when plugged into equation (9), they give rate constants in units of cm^3 s^{-1}. Temperatures in the calculation of $x = \ln(T)$ should be in K. Notice that $(2J_1+1)a_0[1 \rightarrow 2] \approx (2J_2+1)a_0[1 \leftarrow 2]$ due to the principle of detailed balance.

5 ASTROPHYSICAL IMPLICATIONS

The vibrational and rotational distribution of H_3^+ ions in interstellar space, planetary ionospheres and in laboratory is determined by the competition between radiative and collisional processes. While the ionization level is generally low in astrophysical plasmas, electrons can still play a role in the molecular excitation because electron-impact rates exceed those for excitation by neutrals (H, He, H_2) by several orders of magnitude. Detailed excitation models, including collisional data for all relevant colliders, are therefore required to derive reliable column densities from astronomical observations.

An important concept in this context is the so-called critical density, $n_{\rm cr}$, which is defined as the density at which the collisional rate is equal to the spontaneous radiative rate. The usual definition refers to a specific transition in a two-level approach. For a multi-level system, neglecting opacity effects, a practical definition is to refer to a specific level s:

$$n_{\rm cr}(s, T) = \frac{\sum_{s'} A(s \rightarrow s')}{\sum_{s'} \alpha(s \rightarrow s', T)}, \tag{10}$$

where $A(s \rightarrow s')$ are the Einstein coefficients for spontaneous emission, $\alpha(s \rightarrow s', T)$ are the collisional rates and the sums run over all possible transitions $s \rightarrow s'$. Considering electron collisions only, these latter will maintain the level s in local thermodynamic equilibrium (LTE) for electron densities $n_{\rm e} \gg n_{\rm cr}(s, T)$, while deviations from LTE including population inversions are expected for densities $n_{\rm e} \lesssim n_{\rm cr}(s, T)$. For $n_{\rm e} \ll n_{\rm cr}(s, T)$, electron collisions will be negligible. Non-LTE effects caused by H_2 collisions have been investigated both in interstellar clouds (Oka & Epp 2004; Oka et al. 2005) and in the Jovian atmosphere (Melin et al. 2005). We note in this context that microcanonical statistical calculations have been performed recently to estimate thermal state-to-state rate coefficients for the $H_3^+ + H_2$ reaction and its deuterated variants (Park & Light 2007; Hugo, Asvany & Schlemmer 2009). Electron-impact rotational excitation has been considered by Faure et al. (2006b) but, to the best of our knowledge, electron-impact vibrational excitation has been so far ignored in non-LTE modelling.

Equation (10) was computed with the vibrational and rotational rates presented in the previous sections. Einstein A coefficients were taken from Dinelli, Miller & Tennyson (1992a,b) for vibrational transitions and from Pan & Oka (1986) for rotational transitions. Results are presented in Tables 6 and 7. It can be noted that critical densities for vibrational and rotational levels differ by typically six orders of magnitude: they range between 10^7 and 10^{10} cm^{-3} for the former and between 10^{-1} and 10^4 cm^{-3} for the latter. In the diffuse interstellar medium, the electron density is $\sim$0.1 cm^{-3} (Black & van Dishoeck 1991) while it can reach about 10^6 cm^{-3} in planetary atmospheres (see, e.g., Lystrup et al. 2008). As a result, non-LTE rotational populations are expected in interstellar clouds, whereas rotational levels should be at or close to LTE in

Table 2. Parameters a_0, a_1, a_2 and a_3 of the fit polynomial $P_m(x)$ of equation (9) for several transitions between rotational states of the E'' irreducible representation of the coordinate part of the ion–electron system. The vibrational level of the ion is the same in the initial and final states. The upper line specifies the pairs (J_1K_1)–(J_2K_2) of rotational states for which the parameters are fitted. For convenience, we also specify (second line of the table) the threshold energy $\Delta_{r'r}$ for each transition. All but the first rows in the table have two numbers: the upper number in each cell corresponds to the transition $(J_1K_1) \rightarrow (J_2K_2)$, the lower number corresponds to the reverse transition $(J_1K_1) \leftarrow (J_2K_2)$.

	(11)–(21)	(11)–(31)	(21)–(31)	(21)–(41)	(31)–(41)	(31)–(51)	(41)–(51)
$\Delta_{r'r}$(K)	249	619	370	858	488	1087	600
a_0	1.51e−5	2.29e−6	9.47e−6	1.01e−5	3.17e−6	7.04e−6	3.24e−6
	8.81e−6	9.74e−7	6.33e−6	5.18e−6	2.20e−6	4.24e−6	2.41e−6
a_1	4.6e−7	6.13e−7	−3.76e−7	−2.64e−6	−3.43e−7	7.62e−8	−4.56e−7
	4.08e−7	2.72e−7	−2.44e−8	−1.21e−6	−1.17e−7	1.87e−7	−2.31e−7
a_2	−3.96e−7	7.16e−8	−1.14e−7	5.77e−7	1.10e−7	−1.82e−8	4.54e−8
	−2.62e−7	2.83e−8	−1.25e−7	2.74e−7	5.81e−8	−3.69e−8	1.1e−8
a_3	3.00e−8	−1.07e−8	8.57e−9	3.78e−8	−1.09e−8	7.6e−10	−1.94e−9
	1.94e−8	−4.42e−9	8.73e−9	−1.83e−8	6.85e−9	1.99e−9	−2.3e−11

Table 3. Parameters a_i for several transitions between rotational states of the E' irreducible representation of the ionic wavefunction. See Table 2 for details.

	(22)–(32)	(22)–(42)	(32)–(42)	(32)–(52)	(42)–(52)	(44)–(54)
$\Delta_{r'r}$(K)	372	862	490	1092	602	614
a_0	1.39e−5	3.69e−6	8.36e−6	5.94e−6	9.79e−6	1.07e−5
	9.38e−6	1.87e−6	5.99e−6	3.48e−6	7.42e−6	8.01e−6
a_1	−2.73e−6	5.97e−8	−1.34e−6	−5.51e−7	−2.51e−6	−7.78e−8
	−1.66e−6	1.37e−7	−7.52e−7	−1.85e−7	−1.73e−6	3.53e−7
a_2	5.98e−7	−2.38e−8	4.05e−7	8.42e−8	4.69e−7	−1.77e−7
	3.73e−7	−3.22e−8	2.63e−7	2.32e−8	3.25e−7	−2.22e−7
a_3	−4.35e−8	1.53e−9	−3.55e−8	−4.e−9	−3.06e−8	1.6e−8
	−2.79e−8	1.98e−9	−2.46e−8	−7.4e−10	−2.16e−8	1.77e−8

Table 4. The table gives parameters a_i for several transitions between rotational states of the A_2' irreducible representation of the ionic wavefunction. See Table 2 for details.

	(10)–(30)	(30)–(50)
$\Delta_{r'r}$(K)	619	1085
a_0	9.54e−6	6.01e−6
	3.85e−6	3.58e−6
a_1	−3.87e−7	4.14e−8
	−3.32e−8	1.64e−7
a_2	1.43e−7	1.04e−7
	3.71e−8	4.12e−8
a_3	−1.155e−8	−1.06e−8
	−3.50e−9	−5.23e−9

Table 5. The table gives parameters a_i for several transitions between rotational states of the A_2'' irreducible representation of the ionic wavefunction. See Table 2 for details.

	(33)–(43)	(33)–(53)	(43)–(53)
$\Delta_{r'r}$(K)	494	1101	607
a_0	1.39e−5	2.16e−6	1.26e−5
	9.92e−6	1.31e−6	9.84e−6
a_1	−1.34e−6	7.37e−8	−2.07e−6
	−5.56e−7	8.18e−8	−1.41e−6
a_2	4.56e−8	−1.81e−8	3.86e−7
	−5.41e−8	−1.79e−8	2.65e−7
a_3	3.38e−9	1.09e−9	−2.75e−8
	7.95e−9	1.07e−9	−1.95e−8

the Jovian atmosphere. A non-thermal rotational distribution of H_3^+ was actually observed towards Galactic Centre clouds, where the metastable (3, 3) level has a population comparable to that in (1, 1) despite being 361.5 K higher (Oka et al. 2005). On the other hand, electrons are expected to be negligible in vibrationally exciting H_3^+ in the interstellar medium but they could establish a non-LTE vibrational population of H_3^+ in planetary environments, as observed in the Jovian thermosphere (Kim, Fox & Porter 1992).

Table 6 shows that the two levels $\{10^0\}$ and $\{20^0\}$ have critical densities significantly lower than the other levels. This directly reflects the lower Einstein A coefficients of $\sim$1 s^{-1} (Dinelli et al. 1992a). We note that the values are however not low enough to ensure LTE vibrational population in planetary atmospheres where $n_e < 10^7$ cm^{-3}.

Table 7 shows that at 10 K, the levels (22) and (44) have much higher critical densities than the other levels. This actually reflects

Table 6. Critical electron density, n_{cr} in cm^{-3}, at 10, 100 and 1000 K, for vibrational levels of H_3^+. Powers of 10 are given in parentheses.

T	$\{01^1\}$	$\{10^0\}$	$\{02^0\}$	$\{02^2\}$	$\{11^1\}$	$\{20^0\}$	$\{03^1\}$
10	1.3(9)	2.4(7)	3.1(9)	2.6(9)	9.5(8)	4.8(7)	1.3(9)
100	4.0(9)	7.7(7)	9.7(9)	8.1(9)	3.0(9)	1.5(8)	4.2(9)
1000	1.1(10)	2.0(8)	2.3(10)	2.1(10)	8.9(9)	4.8(8)	1.3(10)

Table 7. Critical electron density, n_{cr} in cm^{-3}, at 10, 100 and 1000 K, for several rotational levels of H_3^+ (the levels are grouped according to the corresponding irreducible representations). Powers of 10 are given in parentheses.

T	(21)	(31)	(41)	(51)	(30)	(50)	(43)	(53)	(22)	(32)	(42)	(52)	(44)	(54)
10	2.5(−1)	2.7(1)	4.6(2)	2.4(3)	3.6(1)	2.2(3)	3.6(1)	2.2(3)	3.9(15)	1.3(1)	1.2(2)	1.1(3)	6.4(23)	1.3(1)
100	9.6(−1)	9.4(1)	1.2(3)	7.9(3)	1.1(2)	6.0(3)	6.7(1)	2.0(1)	3.6(1)	4.3(1)	3.8(2)	3.8(3)	2.3(0)	4.8(1)
1000	1.9(0)	1.5(2)	2.5(3)	2.7(4)	2.1(2)	1.8(4)	1.4(2)	7.0(1)	3.5(0)	7.7(1)	9.4(2)	1.3(4)	3.5(-2)	1.8(2)

the fact that these two levels can depopulate collisionally through *excitation* only since rates for rotational transitions with $\Delta K \neq 0$ are null within our treatment. These rates, as those with $|\Delta J| > 2$, were actually estimated by Faure & Tennyson (2003) and Faure et al. (2006a), and were found to be three to four orders of magnitude smaller than those with $\Delta J = \pm 1, \pm 2$ and $\Delta K = 0$. The (44) level is particularly interesting because an astrophysical maser is predicted in the (44)→(31) transition of H_3^+ (Black 2000). It should be noted that the selection rules for the (forbidden) rotational radiative transitions are $\Delta J = 0, \pm 1$ and $\Delta K = \pm 3$ (Pan & Oka 1986; Miller & Tennyson 1988). Critical densities suggest that electrons might contribute, in some environments, to create and maintain the necessary population inversion. Note that in Table 7, the (33) level is not listed since it is metastable. In this case, the concept of critical density is meaningless. Finally, we emphasize that critical densities provide guidance at the order of magnitude level and that a detailed non-LTE modelling, including all relevant colliders, is necessary to properly quantify deviations from LTE.

6 CONCLUSION

In this study, we have performed calculations of thermally averaged rate constants for rotational and vibrational transitions in H_3^+ ion caused by an electron impact. The calculations were made from the first principles using the quantum-defect approach. The rotational rate constants are calculated for the ground vibrational level of the ion in the initial and final states. The rate constants for transitions between different vibrational levels are calculated neglecting the rotational substructure of each vibrational level, which corresponds to averaging over initial rotational states and summing over the final rotational states. The obtained thermally averaged rate constants are well described by the analytical formula of equation (7) with the parameter P_0, that can be considered as temperature independent for vibrational transitions, and weakly dependent on temperature for the rotational transitions. For the rotational transitions, we have made a numerical fit of the parameter by a cubic polynomial. The numerical values of the fitting procedure are provided in Tables 1–5. The presented thermally averaged rate constants can be useful in interpretation of hydrogen-dominated plasma experiments as well as for modelling interstellar clouds and planetary atmospheres, where the H_3^+ ion is present. The computation of critical densities suggests, in particular, that electrons could establish non-LTE rotational populations of H_3^+ in diffuse interstellar clouds and non-LTE vibrational populations in planetary atmospheres.

ACKNOWLEDGMENTS

This work has been supported by the National Science Foundation under grant no. PHY-0855622, by the Department of Energy, Office of Science and by an allocation of NERSC supercomputing resources. Support by the French CNRS National Programme 'Physique et Chimie du Milieu Interstellaire' and the *Réseau thématique de recherches avancées 'Triangle de la Physique'* is acknowledged.

REFERENCES

Atabek O., Jungen C., Dill D., 1974, Phys. Rev. Lett., 33, 123
Aymar M., Greene C. H., Luc-Koenig E., 1996, Rev. Modern Phys., 68, 1015
Black J. H., 2000, Philos. Trans. R. Soc. Lond. A, 358, 2515
Black J. H., van Dishoeck E., 1991, ApJ, 369, L9
Bordas C., Helm H., 1991, Phys. Rev. A, 43, 3645
Dinelli B., Miller S., Tennyson J., 1992a, J. Molecular Spectrosc., 153, 718
Dinelli B., Miller S., Tennyson J., 1992b, J. Molecular Spectrosc., 156, 243
Fano U., 1975, J. Opt. Soc. America, 65, 979
Faure A., Tennyson J., 2002, J. Phys. B: Atomic Molecular Opt. Phys., 35, 3945
Faure A., Tennyson J., 2003, MNRAS, 340, 468
Faure A., Kokoouline V., Greene C. H., Tennyson J., 2006a, J. Phys. B: Atomic Molecular Opt. Phys., 39, 4261
Faure A., Wiesenfeld L., Valiron P., Tennyson J., 2006b, Philos. Trans. R. Soc. Lond. A, 364, 3113
Faure A., Tennyson J., Kokoouline V., Greene C. H., 2009, J. Phys: Conf. Ser., 192, 012016
Fonseca dos Santos S., Kokoouline V., Greene C. H., 2007, J. Chemical Phys., 127, 124309
Gorfinkiel J., Tennyson J., 2004, J. Phys. B: Atomic Molecular Opt. Phys., 37, L343
Hugo E., Asvany O., Schlemmer S., 2009, J. Chemical Phys., 130, 164302
Jimenez-Serra I., Martin-Pintado J., Viti S., Martin S., Rodriguez-Franco A., Faure A., Tennyson J., 2006, ApJ, 650, L135
Johnsen R., 2005, J. Phys: Conf. Ser., 4, 83
Jungen C., Atabek O., 1977, J. Chemical Phys., 66, 5584
Kim Y., Fox J., Porter H., 1992, J. Geophys. Res., 97, 6093
Kokoouline V., Greene C. H., 2003a, Phys. Rev. Lett., 90, 133201

Kokoouline V., Greene C. H., 2003b, Phys. Rev. A, 68, 012703
Kokoouline V., Greene C. H., 2004a, Phys. Rev. A, 69, 032711
Kokoouline V., Greene C. H., 2004b, Faraday Discussion, 127, 413
Kokoouline V., Greene C. H., Esry B. D., 2001, Nat, 412, 891
Larsson M., 2000, Philos. Trans. R. Soc. Lond. A, 358, 2433
Lindsay C., McCall B., 2001, J. Molecular Spectrosc., 210, 60
Lystrup M. B., Miller S., Dello Russo N., Vervack R. J. J., Stallard T., 2008, ApJ, 677, 790
Melin H., Miller S., Stallard T., Grodent D., 2005, Icarus, 178, 97
Miller S., Tennyson J., 1988, ApJ, 335, 486
Miller S. et al., 2000, Philos. Trans. R. Soc. Lond. A, 358, 2485
Mistrík I., Reichle R., Müller U., Helm H., Jungen M., Stephens J., 2000, Phys. Rev. A, 61, 033410
Oka T., 2006, Proc. Natl. Acad. Sci., 103, 12235
Oka T., Epp E., 2004, ApJ, 613, 349
Oka T., Geballe T. R., Goto M., Usuda T., McCall B. J., 2005, ApJ, 632, 882
Pan F.-S., Oka T., 1986, ApJ, 305, 518
Park K., Light J., 2007, J. Chemical Phys., 126, 044305
Plasil R., Glosik J., Poterya V., Kudrna P., Rusz J., Tichy M., Pysanenko A., 2002, Int. J. Mass Spectrometry, 218, 105
Seaton M. J., 1966, Proc. Phys. Soc. Lond., 88, 801
Staib A., Domcke W., 1990, Z. Phys. D, 16, 275
Stephens J. A., Greene C. H., 1994, Phys. Rev. Lett., 72, 1624
Stephens J. A., Greene C. H., 1995, J. Chemical Phys., 102, 1579

This paper has been typeset from a TEX/LATEX file prepared by the author.